

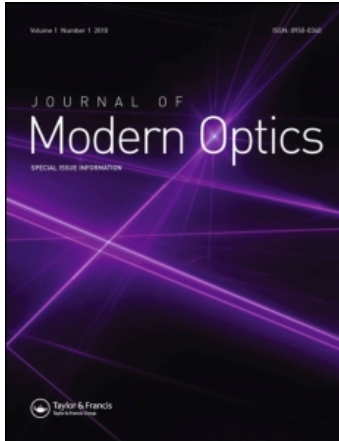
This article was downloaded by: [ULB University of Brussels]

On: 17 July 2010

Access details: Access Details: [subscription number 918147498]

Publisher Taylor & Francis

Informa Ltd Registered in England and Wales Registered Number: 1072954 Registered office: Mortimer House, 37-41 Mortimer Street, London W1T 3JH, UK



## Journal of Modern Optics

Publication details, including instructions for authors and subscription information:

<http://www.informaworld.com/smpp/title~content=t713191304>

### Resolution in Diffraction-limited Imaging, a Singular Value Analysis

M. Bertero<sup>a</sup>; C. De Mol<sup>b</sup>; E. R. Pike<sup>c</sup>; J. G. Walker<sup>c</sup>

<sup>a</sup> Istituto Matematico dell'Università and Istituto Nazionale di Fisica Nucleare, Genoa, Italy. <sup>b</sup>

Département de Mathématique, Université Libre de Bruxelles, Bruxelles, Belgium. <sup>c</sup> Royal Signals and Radar Establishment, Malvern, England.

**To cite this Article** Bertero, M. , De Mol, C. , Pike, E. R. and Walker, J. G.(1984) 'Resolution in Diffraction-limited Imaging, a Singular Value Analysis', Journal of Modern Optics, 31: 8, 923 – 946

**To link to this Article:** DOI: 10.1080/713821597

**URL:** <http://dx.doi.org/10.1080/713821597>

PLEASE SCROLL DOWN FOR ARTICLE

Full terms and conditions of use: <http://www.informaworld.com/terms-and-conditions-of-access.pdf>

This article may be used for research, teaching and private study purposes. Any substantial or systematic reproduction, re-distribution, re-selling, loan or sub-licensing, systematic supply or distribution in any form to anyone is expressly forbidden.

The publisher does not give any warranty express or implied or make any representation that the contents will be complete or accurate or up to date. The accuracy of any instructions, formulae and drug doses should be independently verified with primary sources. The publisher shall not be liable for any loss, actions, claims, proceedings, demand or costs or damages whatsoever or howsoever caused arising directly or indirectly in connection with or arising out of the use of this material.

## Resolution in diffraction-limited imaging, a singular value analysis

### IV. The case of uncertain localization or non-uniform illumination of the object

M. BERTERO

Istituto Matematico dell'Università and  
Istituto Nazionale di Fisica Nucleare, Genoa, Italy

C. DE MOL

Département de Mathématique, Université Libre de Bruxelles,  
Bruxelles, Belgium

E. R. PIKE and J. G. WALKER

Royal Signals and Radar Establishment, Malvern, England

(Received 21 December 1983)

**Abstract.** Previous work in this series, in which the theory of singular systems has been used to discuss the problem of diffraction-limited imaging, is generalized to allow the reconstruction of an object over a region with 'soft' edges. The generalization is introduced to deal with gaussian-beam or other illumination or uncertain *a priori* knowledge of position. The solutions are developed in a weighted  $L^2$  space. Examples of singular functions and vectors with both gaussian and sinc illumination are given. The analysis is applied to determine the amplitude response functions of the scanning optical or acoustic microscope systems proposed by Bertero and Pike in the first paper of the series and it is found that the performance of a scanning microscope of the new type should approach exactly that of a conventional coherent microscope of twice the resolving power.

#### 1. Introduction

This is the fourth paper of a series [1-3] in which diffraction-limited imaging is treated by singular value analysis. The theory of singular systems is an extension of the mathematical technique of eigenfunction decomposition which has been the principal tool in previous treatments of this problem, as given for example by Toraldo di Francia [4]. When the object and image domains are allowed to differ, and in particular if the object domain is small and the image is known over a region much larger than the object domain, it is possible to prove by means of singular value techniques that such information may be used to improve resolution beyond that predicted by the 'classical' accepted theory.

This was demonstrated in [1] for coherent illumination and in [2] for incoherent illumination, where the *a priori* support of the object was  $[-X/2, X/2]$  and the image was assumed to be known as a continuous function in  $(-\infty, +\infty)$ . In [3] this work was extended to the more practical situation where the image is known only on a

finite set of sampled points over a truncated region, and the singular value analysis was shown to be sufficiently powerful to accommodate this case in a general theory. The object was again known *a priori* to be supported on  $[-X/2, X/2]$ .

There are two situations, however, where our *a priori* knowledge of an object support with 'hard boundaries' is not applicable, but yet where extra information about its localization is available and may be used, in the spirit of the singular value approach, to increase the resolution of a reconstructed object. The first is when the object, although possibly of unknown support, is illuminated non-uniformly, the illumination tending to zero away from the centre of the beam. Reconstruction over a finite region with 'soft edges' is then required; a commonly occurring example is a gaussian illumination profile. The second situation arises where an *a priori* estimate of the object profile is available. For example, a bright region in a low-resolution image might justify inspection at higher resolution, and the low-resolution image itself might be used as an *a priori* estimate. Alternatively, an imprecise knowledge of an object's position might be treated by taking a gaussian or other function, concentrated near a fixed point, as a suitable prior estimate.

In both these cases the theory of singular systems presented in the previous papers of this series may be used with a suitable generalization, taking into account a 'profile function'  $P$ , which may be interpreted in either of the two ways discussed above. In this paper we take the view that the object to be reconstructed is that which exists independently of the illumination or *a priori* estimate. The results will also allow us to develop a solution where the object is defined by its product with the profile; we will not discuss this case here.

For one-dimensional coherent illumination, the basic equation is

$$g(x) = \int_{-\infty}^{+\infty} \frac{\sin[\Omega(x-y)]}{\pi(x-y)} P(y)f(y) dy, \quad (1.1)$$

where  $f(y)$  is the object 'transparency' and the notation conforms to that of the previous papers. Thus [1-3] for uniform illumination

$$P(y) = \begin{cases} 1, & |y| < X/2 \\ 0, & |y| > X/2 \end{cases} \quad (1.2)$$

For gaussian illumination

$$P(y) = \exp(-y^2/2\beta^2) \quad (1.3)$$

and for illumination by a uniformly filled lens of the same aperture as the imaging instrument

$$P(y) = \frac{\sin(\Omega y)}{\Omega y} = \text{sinc}(\Omega y). \quad (1.4)$$

We scale the profile function such that

$$|P(y)| \leq 1. \quad (1.5)$$

Equation (1.1) is a Fredholm integral equation of the first kind and has a rather general structure; it is also encountered in other problems.

Let us consider the equation

$$g(x) = \int_a^b T(x, y)f(y) dy, \quad c \leq x \leq d. \quad (1.6)$$

In many problems we can assume that  $f \in L^2(a, b)$  and that the kernel  $T(x, y)$  satisfies conditions such that equation (1.6) defines a compact transformation of  $L^2(a, b)$  into  $L^2(c, d)$ . In these cases the solution of the inverse problem is ill-posed. The condition of compactness excludes the case of convolution operators, but these can be easily treated by Fourier transform techniques. The singular value analysis described in the previous papers in this series, and also in a parallel series in the Laplace transform [5–7], takes advantage of *a priori* knowledge of a smaller support of  $f$ , say  $[a', b']$ , to restrict the operator of equation (1.6) to the Hilbert space  $L^2(a', b')$ . We generalize this approach here by taking a weighted  $L^2$ -space for the space of solutions. We define a norm of  $f$  as

$$\|f\|^2 = \int_a^b \frac{|f(y)|^2}{|P(y)|^2} dy < +\infty. \quad (1.7)$$

By making the assignment  $f \leftarrow Pf$ , equation (1.6) with  $f$  satisfying equation (1.7), becomes equivalent to

$$g(x) = \int_a^b T(x, y)P(y)f(y) dy, \quad c \leq x \leq d \quad (1.8)$$

with  $f$  square-integrable:

$$\|f\|^2 = \int_a^b |f(y)|^2 dy < +\infty. \quad (1.9)$$

Clearly equation (1.8) has the same structure as that of equation (1.1), but  $P(y)$  now has the significance of a general weighting function.

In order to apply singular value methods to the solution of equation (1.8), we introduce the integral operator

$$(Kf)(x) = \int_a^b T(x, y)P(y)f(y) dy, \quad c \leq x \leq d \quad (1.10)$$

as an operator from  $L^2(a, b)$  into  $L^2(c, d)$ . The adjoint  $K^*$  is given by

$$(K^*g)(y) = P^*(y) \int_c^d T^*(x, y)g(x) dx, \quad a \leq y \leq b. \quad (1.11)$$

The operators  $K^*K$  and  $KK^*$  are integral operators (the first in  $L^2(a, b)$  and the second in  $L^2(c, d)$ ) whose kernels are given, respectively, by

$$S(y, y') = P^*(y)P(y') \int_c^d T^*(x, y)T(x, y') dx, \quad (1.12)$$

$$U(x, x') = \int_a^b T(x, y)|P(y)|^2 T^*(x', y) dy. \quad (1.13)$$

In order to have a compact operator  $K$ , and consequently to be able to apply the singular value analysis to equation (1.8), it is sufficient to require that the kernel  $S(y, y')$  or the kernel  $U(x, x')$  be square-integrable.

In § 2 we first obtain some general properties of the singular system of equation (1.1) without specifying any particular profile function; then, in § 3 we consider the special case where  $P(y)$  is gaussian. In § 4 we revert to the general case, but with discrete data and in § 5 we present some numerical results by which the effects of

uniform, gaussian and sinc profile functions are compared. In §6 we give details for extending the theory to two dimensions, and in §7 we discuss applications to scanning microscopy. A general conclusion is that, the more broadly spread the profile function, the lower will be the resolution achievable; this shows up in the analysis as a 'leaking-out' of zeros of the singular functions from the central region. For a band-limited profile function the density of zeros saturates at a fixed value, no matter how high up the singular function series we go, and this—in microscopy—places a limitation on super-resolution that was described in broader terms by McCutchen [8] some years ago†.

Work of a similar but complementary nature to that of the present paper has been undertaken by Luttrell [9] and will be published independently.

## 2. The one-dimensional problem: general properties of singular values and singular functions

Here we derive the main properties of the integral operator defined by equation (1.1), namely

$$(Af)(x) = \int_{-\infty}^{+\infty} \frac{\sin[\Omega(x-y)]}{\pi(x-y)} P(y)f(y) dy. \quad (2.1)$$

We assume that the support of the profile function  $P(y)$  is  $(-\infty, +\infty)$ , that  $P(y)$  is normalized in order to satisfy condition (1.5), and furthermore that it is square-integrable:

$$\int_{-\infty}^{+\infty} P^2(y) dy < +\infty. \quad (2.2)$$

All these conditions are satisfied by the profile functions (1.3) and (1.4).

Then, if we assume that the 'transparency' of the object is square-integrable, equation (7.1) defines a linear, compact operator in  $L^2(-\infty, +\infty)$ . This property is easily verified since, if we introduce the kernel

$$K(x, y) = \frac{\sin[\Omega(x-y)]}{(x-y)} P(y), \quad (2.3)$$

then  $K(x, y)$  is square-integrable:

$$\begin{aligned} \iint_{-\infty}^{+\infty} |K(x, y)|^2 dx dy &= \left( \int_{-\infty}^{+\infty} \frac{\sin^2(\Omega\xi)}{\pi^2\xi^2} d\xi \right) \left( \int_{-\infty}^{+\infty} |P(y)|^2 dy \right) \\ &\equiv \frac{\Omega}{\pi} \int_{-\infty}^{+\infty} |P(y)|^2 dy < +\infty; \end{aligned} \quad (2.4)$$

therefore the operator  $A$  is of the Hilbert-Schmidt class.

With regard to the invertibility of the operator  $A$ , the following results cover all cases of practical interest: if  $\hat{P}(\omega)$ , the Fourier transform of  $P(y)$ , has a bounded support, then the operator  $A$  is not injective, namely the equation  $Af=0$  has non-trivial solutions  $f \neq 0$ ; on the other hand, if  $\hat{P}(\omega)$  is analytic, then the operator  $A$  is injective.

†The comment made in Bertero and Pike [1] on this work was incorrect and is unreservedly withdrawn.

The proof is quite simple and is based on the following remark: if we write  $g = Af$  and take the Fourier transform of both sides, then since  $Af = 0$  we obtain

$$\hat{g}(\omega) = \int_{-\infty}^{+\infty} \hat{P}(\omega - \mu) \hat{f}(\mu) d\mu = 0, \quad |\omega| < \Omega. \quad (2.5)$$

Now, if the support of  $\hat{P}(\omega)$  is interior to the interval  $[-\omega_0, \omega_0]$ , in equation (2.5) we have contributions only from the values of  $\hat{f}$  corresponding to the interval  $J_0 = [-(\omega_0 + \Omega), \omega_0 + \Omega]$ . Therefore if  $\hat{f}(\omega)$  is zero on  $J_0$  but non-zero elsewhere, then  $Af = 0$  without having  $f = 0$ , and  $A$  is not injective.

On the other hand, if  $\hat{P}(\omega)$  is analytic, then  $\hat{g}(\omega)$  in equation (2.5) is also analytic and therefore if it is zero for  $|\omega| < \Omega$ , it is zero everywhere. It follows that  $Pf = 0$  and therefore that  $f = 0$ , since we have assumed that the support of  $P$  is  $(-\infty, +\infty)$ .

These results imply that the operator  $A$  is injective for a gaussian profile (equation (1.3)), but not for a sinc profile (equation (1.4)). For the sinc profile one can also obtain a more precise result. Indeed, starting from equation (2.5) and noting that now  $\hat{P}(\omega) = 1$ ,  $|\omega| \leq \Omega$  and  $\hat{P}(\omega) = 0$ ,  $|\omega| > \Omega$  one can prove that  $\hat{g}(\omega) = 0$  if and only if  $\hat{f}(\omega) = 0$  when  $|\omega| < 2\Omega$  or  $\hat{f}(\omega)$  is the restriction to the interval  $[-2\Omega, 2\Omega]$  of a periodic function of period  $2\Omega$  and such that the integral over the period is zero. From this result and from the sampling theorem it follows that the orthogonal complement of the null space of the operator  $A$  is just the space of the band-limited functions, with band  $[-2\Omega, 2\Omega]$ , which are zero at the sampling points  $n\pi/\Omega$  ( $n = \pm 1, \pm 2, \dots$ ), namely the zeros of the profile function. The  $u_k$ s form an orthonormal basis in this space and we shall use this property in deriving the impulse response of a scanning microscope in § 7.

We now introduce the adjoint operator  $A^*$ , defined such that

$$(A^*g)(y) = P^*(y) \int_{-\infty}^{+\infty} \frac{\sin[\Omega(x-y)]}{\pi(x-y)} g(x) dx. \quad (2.6)$$

The singular system  $\{\alpha_k; u_k, v_k\}_{k=0}^{+\infty}$  of the operator  $A$  is then the set of the non-trivial solutions of the coupled equations

$$Au_k = \alpha_k v_k, \quad A^*v_k = \alpha_k u_k \quad (2.7)$$

where  $\alpha_k > 0$ . If the operator  $A$  is injective, then the set  $\{u_k\}_{k=0}^{+\infty}$  is an orthogonal basis in  $L^2(-\infty, +\infty)$ ; otherwise it is a basis in the orthogonal complement of the null space of  $A$ . Analogously, the set  $\{v_k\}_{k=0}^{+\infty}$  is a basis in the orthogonal complement of the null space of  $A^*$ , namely the subspace  $B_\Omega$  of the band-limited functions with the band  $[-\Omega, \Omega]$ .

If we write equations (2.7) explicitly, we obtain

$$\int_{-\infty}^{+\infty} \frac{\sin[\Omega(x-y)]}{\pi(x-y)} P(y) u_k(y) dy = \alpha_k v_k(x), \quad (2.8)$$

$$P^*(y) \int_{-\infty}^{+\infty} \frac{\sin[\Omega(x-y)]}{\pi(x-y)} v_k(x) dx = \alpha_k u_k(y). \quad (2.9)$$

We note that there exists a very simple relation between the singular functions  $u_k$  and the singular functions  $v_k$ . Indeed, from equation (2.8) it follows that  $v_k$  is band-

limited and therefore, since the sinc kernel is just the kernel of the projection operator over  $B_\Omega$ , from equation (2.9) we obtain

$$u_k(y) = \frac{1}{\alpha_k} P^*(y) v_k(y). \tag{2.10}$$

This relation has several implications. Firstly, if we remark that, from the normalization condition of the functions  $v_k$  we have

$$\begin{aligned} |v_k(y)| &= \left| \frac{1}{2\pi} \int_{-\Omega}^{\Omega} \hat{v}_k(\omega) \exp(iy\omega) d\omega \right| \\ &\leq \sqrt{\frac{\Omega}{\pi}} \left( \frac{1}{2\pi} \int_{-\Omega}^{\Omega} |\hat{v}_k(\omega)|^2 d\omega \right)^{1/2} = \sqrt{\left(\frac{\Omega}{\pi}\right)} \end{aligned} \tag{2.11}$$

(where Schwarz's inequality has been used), we obtain as the bound for  $u_k(y)$

$$|u_k(y)| \leq \frac{1}{\alpha_k} \sqrt{\left(\frac{\Omega}{\pi}\right)} |P(y)|. \tag{2.12}$$

In particular, the zeros of  $P(y)$  are also zeros of any  $u_k(y)$ .

Secondly, from the orthonormality conditions of the functions  $u_k$  and  $v_k$  we obtain the following relations for the functions  $v_k$  as

$$\int_{-\infty}^{+\infty} v_k(x) v_j^*(x) dx = \delta_{kj}, \tag{2.13}$$

$$\int_{-\infty}^{+\infty} |P(x)|^2 v_k(x) v_j^*(x) dx = \alpha_k^2 \delta_{kj}. \tag{2.14}$$

In other words, the singular functions  $v_k$  have a double orthogonality property which is a generalization of the well-known double orthogonality of the linear prolate spheroidal functions.

Finally, if  $P$  is band-limited, then the  $u_k$ s are also band-limited. In particular, in the case of the sinc profile (equation (1.4)), the band of the  $u_k$ s is the interval  $[-2\Omega, 2\Omega]$ .

The singular functions  $u_k$  are also solutions of the eigenvalue problem

$$A^* A u_k = \alpha_k^2 u_k, \tag{2.15}$$

which can be written explicitly as

$$\int_{-\infty}^{+\infty} P^*(y) \frac{\sin[\Omega(y-y')]}{\pi(y-y')} P(y') u_k(y') dy' = \alpha_k^2 u_k(y). \tag{2.16}$$

Similarly, the singular functions  $v_k$  are also solutions of the eigenvalue problem

$$A A^* v_k = \alpha_k^2 v_k, \tag{2.17}$$

which is most conveniently expressed in Fourier space. Indeed, by introducing the relation (2.10) into equation (2.8) and by Fourier-transforming both members of the resulting equation, we obtain

$$\int_{-\Omega}^{\Omega} Q(\omega - \omega') \hat{v}_k(\omega') d\omega' = \alpha_k^2 \hat{v}_k(\omega), \quad |\omega| \leq \Omega, \tag{2.18}$$

where

$$Q(\omega) = \frac{1}{2\pi} \int_{-\infty}^{+\infty} |P(y)|^2 \exp(-i\omega y) dy. \quad (2.19)$$

The interesting feature of equation (2.18) is that it appears as an eigenvalue problem for a Töplitz operator. Indeed, many features of the eigenvalues of such an operator can be deduced from the properties of the Fourier transform of the kernel, which in this case is

$$\hat{Q}(y) = \int_{-\infty}^{+\infty} Q(\omega) \exp(-i\omega y) d\omega = |P(y)|^2. \quad (2.20)$$

Therefore many features of the singular values of the operator (2.1) can be deduced directly from the behaviour of the profile function  $P(y)$ .

A first result is that if the profile function  $P(y)$  satisfies the condition

$$y \frac{d|P(y)|}{dy} \leq 0 \quad (2.21)$$

(or  $\geq 0$ ) for any  $y$ , then all the eigenvalues  $\alpha_k^2$  are non-degenerate (i.e. with a multiplicity of 1). The proof of this result is given by Gori and Palma [10]. We note that the condition (2.21) is satisfied for gaussian illumination, where  $P(y) = \exp(-y^2/2\beta^2)$ , but not for sinc illumination, where  $P(y) = \text{sinc}(\Omega y)$ .

A second result concerns the asymptotic distribution of the eigenvalues  $\alpha_k^2$  when the aperture  $\Omega$  of the imaging system is large. The proof is given elsewhere [11, 12]. Let  $N_\Omega(a, b)$  denote the number of eigenvalues  $\alpha_k^2$  falling within  $(a, b)$ ; that is, satisfying the conditions  $a < \alpha_k^2 < b$ ; if  $a > 0$ ,  $b < 1$  and if  $m(a, b)$  is the measure of the set of values of  $y$  where  $a < |P(y)|^2 < b$ , then

$$\lim_{\Omega \rightarrow \infty} \frac{1}{2\Omega} N(a, b) = \frac{1}{2\pi} m(a, b). \quad (2.22)$$

This relation will be applied to gaussian illumination in the next section.

### 3. Number of degrees of freedom for gaussian illumination

For gaussian illumination it is convenient to introduce the variables

$$t = x/\beta, \quad s = y/\beta, \quad c = \beta\Omega, \quad (3.1)$$

where  $\beta$  is the half-width of the gaussian beam, and the assignments

$$g(\beta t) \rightarrow g(t), \quad \beta f(\beta s) \rightarrow f(s), \quad (3.2)$$

so that the integral equation (1.1) again has the form  $g = Af$ , the integral operator  $A$  being given by

$$(Af)(t) = \int_{-\infty}^{+\infty} \frac{\sin[c(t-s)]}{\pi(t-s)} \exp(-\frac{1}{2}s^2) f(s) dy. \quad (3.3)$$

We intend to compare the distribution of the singular values of the operator (3.3) with the distribution of the singular values of the operator corresponding to the uniform illumination (1.2), which we write, as usual, in the form

$$(Kf)(t) = \int_{-1}^1 \frac{\sin[c(t-s)]}{\pi(t-s)} f(s) ds, \quad -\infty < t < +\infty, \quad (3.4)$$

where

$$c = X\Omega/2. \quad (3.5)$$

As shown in [1], the singular values of  $K$  are just the square roots of the eigenvalues of the linear prolate spheroidal functions.

Using the variables defined in equations (3.1)–(3.3), the eigenvalue equation (2.18) now takes the explicit form

$$\frac{1}{\sqrt{4\pi}} \int_{-c}^c \exp [-(\omega - \omega')^2/4] \hat{v}_k(\omega') d\omega' = \alpha_k^2 \hat{v}_k(\omega), \quad |\omega| \leq c. \tag{3.6}$$

As already remarked in § 2, all the eigenvalues of equation (3.6) are non-degenerate; furthermore, the asymptotic distribution when  $c$  is large is given by equation (2.22) (with  $\Omega$  replaced by  $c$ ).

If we note that in the present case  $\hat{Q}(y) = \exp(-y^2)$  is an even function of  $y$ , the set of the values of  $y$  for which  $a < \hat{Q}(y) < b$  is the union of two intervals,  $(y_b, y_a)$  and  $(-y_a, -y_b)$ , provided  $a < 1$ ; otherwise the set is empty and  $m(a, b) = 0$ . In other words, when  $c$  is large, no singular value of  $A$  can be greater than unity. It is easy to prove that this result holds true, not only for large values of  $c$ , but also for any value of  $c$ .

If we assume that  $0 < a < b < 1$ , then

$$m(a, b) = 2(y_a - y_b) = 2(\sqrt{|\ln a|} - \sqrt{|\ln b|}) \tag{3.7}$$

and therefore, when  $c$  is large,

$$N_c(a, b) \sim \frac{2c}{\pi} (y_a - y_b). \tag{3.8}$$

If we require only one eigenvalue to fall within the interval  $(a, b)$ , then from equation (3.8) we obtain

$$y_a - y_b \sim \pi/2c. \tag{3.9}$$

Clearly the length of the interval  $(y_b, y_a)$  tends to zero when  $c$  tends to infinity, and therefore the length of the interval  $(a, b)$  also tends to zero. As a consequence we obtain the following approximate expression for the eigenvalues  $\alpha_k^2$ , valid when  $c$  is large:

$$\alpha_k^2 \sim \hat{Q}\left(\frac{\pi}{2c} k\right) = \exp\left[-\left(\frac{\pi}{2c}\right)^2 k^2\right]. \tag{3.10}$$

As already remarked, since the function  $\hat{Q}(y)$  satisfies the condition  $\hat{Q}(y) \leq 1$ , all the eigenvalues  $\alpha_k^2$  also satisfy the condition  $\alpha_k^2 \leq 1$ ; furthermore, the greatest eigenvalue  $\alpha_0^2 \rightarrow 1$  from below when  $c \rightarrow \infty$ .

We remark that the asymptotic behaviour of the singular values of the operator  $A$ , (equation (3.3)), namely

$$\alpha_k \sim \exp\left[-\frac{1}{2}\left(\frac{\pi}{2c}\right)^2 k^2\right], \tag{3.11}$$

does not coincide with the asymptotic behaviour of the singular values of the operator  $K$  (equation (3.4)). Indeed, the singular values of  $K$  are the square roots of the eigenvalues of the linear prolate spheroidal functions  $\lambda_k$  [1] and, as it is well known, the  $\lambda_k$  have, for large  $c$ , a step behaviour. This result is not surprising. Indeed,

it is possible to derive the following general expression for the asymptotic behaviour of the singular values of the operator (1.1) when  $\Omega$  is large:

$$\alpha_k \sim \left| P \left( \frac{\pi k}{2\Omega} \right) \right|, \quad (3.12)$$

and therefore a very simple relation exists between the distribution of the singular values and the profile of the illuminating beam.

From equation (3.11) it is easy to derive the number of degrees of freedom of the image, the number  $N_0$  of singular values satisfying the condition

$$\alpha_k \geq \varepsilon/E, \quad (3.13)$$

where  $\varepsilon^2$  and  $E^2$  are the power spectra of the noise and the object, respectively (in the notation of [1]). Since  $\alpha_{N_0} \sim \varepsilon/E$ ,

$$N_0 \sim S\sqrt{2 \ln(E/\varepsilon)}, \quad (3.14)$$

where  $S = 2c/\pi$  is the Shannon number. We point out that for objects illuminated by a gaussian beam, as follows from equation (3.14), the number of degrees of freedom is rather strongly dependent on the signal-to-noise ratio  $E/\varepsilon$ . There is not such a strong dependence for uniform illumination, for which the imaging is described by the integral operator (3.4). Indeed, when  $c$  and  $k$  are large, the asymptotic behaviour for the eigenvalues  $\lambda_k$  of the linear prolate spheroidal functions [13] is described by the relation

$$\lambda_k \sim \frac{1}{1 + \exp(\pi b)}, \quad (3.15)$$

provided

$$k = S + \frac{2}{\pi} b \ln \sqrt{(2\pi S)} \quad (3.16)$$

Then, since  $\alpha_{N_0} = \sqrt{\lambda_{N_0}} \sim \varepsilon/E$ , we obtain  $\pi b \sim 2 \ln(E/\varepsilon)$  and, from equation (3.14),

$$N_0 \sim S + \left( \frac{2}{\pi} \right)^2 \ln \sqrt{(2\pi S)} \ln(E/\varepsilon). \quad (3.17)$$

By comparing equations (3.14) and (3.17) we see that, when  $S$  is large, a tenfold improvement in the signal-to-noise ratio  $E/\varepsilon$  produces a much greater improvement in the number of degrees of freedom corresponding to gaussian illumination than in the number of degrees of freedom corresponding to uniform illumination. However, there is no comparable improvement in resolution, as follows from the distribution of the zeros of the  $u_k$ , determined in § 5, and in particular from the 'saturation' of the zeros inside the central region.

We conclude this section by comparing in table 1, for  $c = 10$ , the singular values  $\alpha_k$ , as computed by the method described in § 5 and from the asymptotic expression (3.11).

Table 1. Comparison of the singular values  $\alpha_k$  of the integral operator (3.3) for  $c=10$ , calculated numerically (see §5) and from the asymptotic expression (3.11).

$k$	$\alpha_k$	
	Calculated numerically	$\exp\left[-\frac{1}{2}\left(\frac{\pi}{2c}\right)^2 k^2\right]$
0	0.98953	1.000
1	0.95878	0.98774
2	0.90970	0.95185
3	0.84529	0.89494
4	0.76932	0.82087
5	0.68592	0.73460
6	0.59926	0.64138
7	0.51310	0.54634
8	0.43073	0.45404
9	0.35461	0.36814
10	0.28642	0.29121
11	0.22704	0.22475
12	0.17671	0.16922
13	0.13508	0.12431
14	0.10147	0.08909
15	0.07492	0.06230

**4. The one-dimensional problem with discrete data**

We assume now, as in [3], that the image  $g(x)$  is given only on a finite set of equidistant points

$$x_n = n\sigma; \quad n = 0, \pm 1, \dots, \pm N, \tag{4.1}$$

where  $\sigma \leq \sigma_0 = \pi/\Omega$  (the Nyquist sampling distance). We then introduce the notation

$$\phi_n(\Omega, \sigma; y) = \frac{\sin[\Omega(y - n\sigma)]}{\pi(\Omega - n\sigma)} \tag{4.2}$$

and we define the operator  $A_N$  by the equation

$$(A_N f)(n\sigma) = \int_{-\infty}^{+\infty} \phi_n(\Omega, \sigma; y) P(y) f(y) dy, \quad n = 0, \pm 1, \dots, \pm N, \tag{4.3}$$

which transforms a function  $f \in L^2(-\infty, +\infty) = X$  into a vector in a  $(2N + 1)$ -dimensional space, namely the vector whose components are the values of the noiseless image at the points  $x_n$ . We denote by  $Y_N$  the range of  $A_N$  and call any element of this space an image vector. As in [3], we introduce in  $Y_N$  the scalar product

$$(g, h)_N = \sigma \sum_{n=-N}^N g(n\sigma) h^*(n\sigma). \tag{4.4}$$

The adjoint operator  $A_N^*$ , transforming a vector of  $Y_N$  into a function of  $X = L^2(-\infty, +\infty)$ , is then given by

$$(A_N^* g)(y) = \sigma \sum_{n=-N}^N g(n\sigma) \phi_n(\Omega, \sigma; y) P(y). \tag{4.5}$$

By definition, the singular system  $\{\alpha_{N,k}; u_{N,k}, v_{N,k}\}_{k=0}^{2N}$  of the operator  $A_N$  is the set of solutions of the coupled equations

$$A_N u_{N,k} = \alpha_{N,k} v_{N,k}, \quad A_N^* v_{N,k} = \alpha_{N,k} u_{N,k}, \tag{4.6}$$

analogous to equations (2.7). The singular functions  $u_{N,k}$  are also the eigenfunctions, associated with the eigenvalues  $\alpha_{N,k}^2$ , of the finite-rank integral operator  $A_N^* A_N$ :

$$(A_N^* A_N f)(y) = \int_{-\infty}^{+\infty} T_N(y, y') f(y') dy', \tag{4.7}$$

where

$$T_N(y, y') = \sigma P^*(y) \sum_{m=-N}^N \phi_n(\Omega, \sigma; y) \phi_n(\Omega, \sigma; y') P(y'). \tag{4.8}$$

On the other hand, the singular vectors  $v_{N,k}$  are also the eigenvectors, associated again with the eigenvalues  $\alpha_{N,k}^2$ , of the  $(2N+1) \times (2N+1)$  matrix  $A_N A_N^*$ :

$$(A_N A_N^* g)(n\sigma) = \sum_{m=-N}^N k_{nm} g(m\sigma), \tag{4.9}$$

where

$$k_{nm} = \int_{-\infty}^{+\infty} \phi_n(\Omega, \sigma; y) |P(y)|^2 \phi_m(\Omega, \sigma; y) dy. \tag{4.10}$$

Using essentially the same methods as developed in [3] one can prove that, when  $N \rightarrow +\infty$  with  $\sigma$  fixed, satisfying the condition  $\sigma \leq \pi/\Omega$ , then, for any fixed  $k$

$$\lim_{N \rightarrow \infty} \alpha_{N,k} = \alpha_k, \tag{4.11}$$

$$\lim_{N \rightarrow \infty} \|u_{N,k} - u_k\|_X = 0 \tag{4.12}$$

$$\lim_{N \rightarrow \infty} v_{N,k}(n\sigma) = v_k(n\sigma) \tag{4.13}$$

where  $\alpha_k$ ,  $u_k$  and  $v_k$  are the singular values and singular functions of the operator  $A$ , (equation (2.1)). We recall that both the singular values  $\alpha_k$  of  $A$  and the singular values  $\alpha_{N,k}$  of  $A_N$  are ordered to form decreasing sequences, and therefore the singular values  $\alpha_{N,k}$  and  $\alpha_k$ , which are compared in equation (4.11), are the singular values having the same position in these sequences. Furthermore, in equation (4.13),  $v_{N,k}(n\sigma)$  denotes the  $n$ -th component of the singular vector  $v_{N,k}$ , while  $v_k(n\sigma)$  is the value at the point  $x_n = n\sigma$  of the singular function  $v_k$  of  $A$ .

The proof of these results follows from the remark that if we introduce the function

$$T(y, y') = P^*(y) \frac{\sin[\Omega(y-y')]}{\pi(y-y')} P(y'), \tag{4.14}$$

which is the kernel of the operator  $A^* A$  (equation (2.16)), and if we use the expansion [14]

$$\frac{\sin[\Omega(y-y')]}{\pi(y-y')} = \sigma \sum_{n=-\infty}^{+\infty} \phi_n(\Omega, \sigma; y) \phi_n(\Omega, \sigma; y'), \tag{4.15}$$

which is uniformly convergent with respect to  $y, y'$  in any bounded domain of  $\mathfrak{R}^2$ , and also the condition (2.2), we can deduce that

$$\lim_{N \rightarrow \infty} \int_{-x}^{+\infty} |T(y, y') - T_N(y, y')|^2 dy dy' = 0. \quad (4.16)$$

Therefore the finite-rank integral operator  $A_N^* A_N$  converges, in the sense of the operator norm of the bounded operators in  $X = L^2(-\infty, +\infty)$ , to the integral operator  $A^* A$ . Then the results (4.11)–(4.13) can be derived, as in [3], using methods borrowed from the perturbation theory of linear operators.

We can conclude, as in the analysis of uniform illumination in [3], that the greatest singular values and the corresponding singular functions of the problem with continuous data can be approximated by the singular values and singular functions of the problem with discrete data.

## 5. Numerical results

We have computed the singular values  $\alpha_k$  and the singular functions  $u_k$  of the integral operator (1.1) for both gaussian and sinc illumination. The numerical method is the same as described in [3]. The kernel of the integral operator  $A^* A$  is approximated by a tensor product of splines, and the eigenvalues and eigenvectors of the resulting matrix are computed by combining the power method and the deflation method.

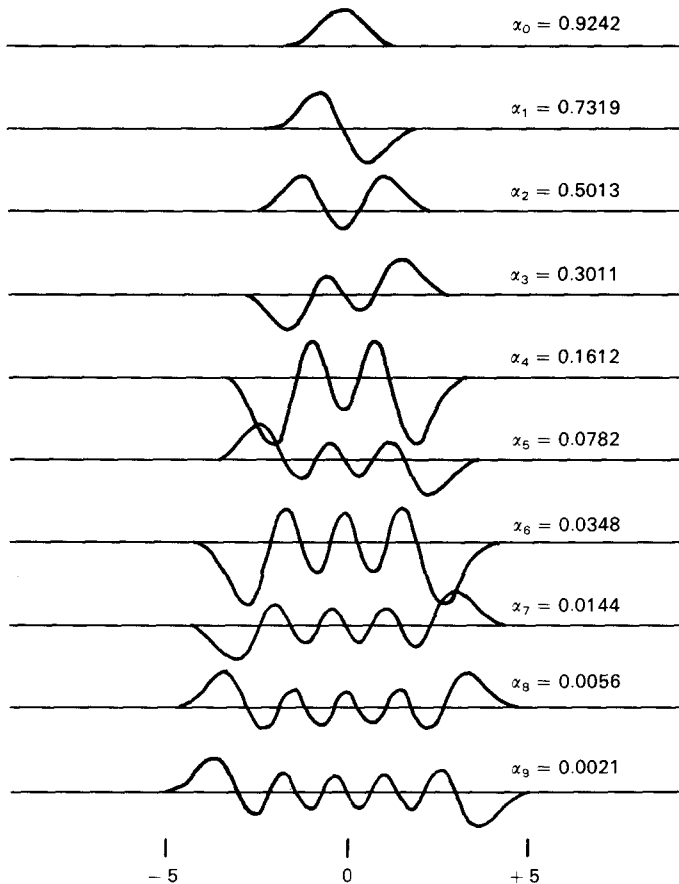
In the present case the integration interval is not bounded. However, this is not a serious difficulty, at least for gaussian illumination. Indeed, the integral appearing in equation (3.3) is rapidly convergent, thanks to the exponential factor, and we can restrict the integration to a rather small interval, for instance  $[-5, 5]$ , in which case the value of the exponential factor at the edges of the interval is of the order of  $10^{-6}$ . This approximation is good for the computation of the first singular values and of the corresponding singular functions  $u_k$ . More accuracy is required for the singular functions corresponding to very small singular values since, as we show, for increasing  $k$  the  $u_k$ s tend to expand out of the central region of the illuminating beam.

In table 2 we give the singular values of the operator (3.3) for small values of the parameter  $c$ , which is the analogue of the space–bandwidth product (also denoted by  $c$ ) for uniform illumination. A comparison of these singular values with the square roots of the eigenvalues of the linear prolate spheroidal functions [15] shows, also for small values of  $c$ , the effect already discussed at the end of §3 for large values of  $c$ . The number of degrees of freedom for gaussian illumination is greater than the number of degrees of freedom for uniform illumination with the same value of  $c$ . However, this increase in the number of degrees of freedom does not lead to any increase in resolution, as is evident from an inspection of the singular functions.

In figures 1 and 2 we give the singular functions  $u_k$  corresponding to the first ten singular values for  $c = \pi$  and  $c = 2\pi$ , respectively. The value  $c = \pi$  corresponds to the half-width of the gaussian beam being equal to the Rayleigh distance of the instrument. Similarly, the value  $c = 2\pi$  corresponds to a half-width of twice the Rayleigh distance. As is already evident for  $c = 2\pi$ , and even more so for higher values of  $c$ , the main lobes of the singular functions corresponding to small singular values tend to move away from the central region of the beam. A similar effect occurs for sinc illumination, and is explained at the end of this section. As a consequence there is a 'saturation' of the number of zeros in the central region of the beam. The average

Table 2. Singular values of the integral operator (3.3) (gaussian illumination) for various values of  $c$  (equation (3.1)).

	$c$			
	1	2	3	4
$\alpha_0$	$6.9852 \times 10^{-1}$	$8.5779 \times 10^{-1}$	$9.1936 \times 10^{-1}$	$9.4845 \times 10^{-1}$
$\alpha_1$	$2.6685 \times 10^{-1}$	$5.4989 \times 10^{-1}$	$7.1689 \times 10^{-1}$	$8.1009 \times 10^{-1}$
$\alpha_2$	$6.9489 \times 10^{-2}$	$2.7491 \times 10^{-1}$	$4.7904 \times 10^{-1}$	$6.2516 \times 10^{-1}$
$\alpha_3$	$1.4429 \times 10^{-2}$	$1.1319 \times 10^{-1}$	$2.7876 \times 10^{-1}$	$4.3828 \times 10^{-1}$
$\alpha_4$	$2.5736 \times 10^{-3}$	$4.0258 \times 10^{-2}$	$1.4397 \times 10^{-1}$	$2.8115 \times 10^{-1}$
$\alpha_5$	$4.0917 \times 10^{-4}$	$1.2779 \times 10^{-2}$	$6.7222 \times 10^{-2}$	$1.6639 \times 10^{-1}$
$\alpha_6$	$5.9281 \times 10^{-5}$	$3.6990 \times 10^{-3}$	$2.8811 \times 10^{-2}$	$9.1605 \times 10^{-2}$
$\alpha_7$	—	$9.9059 \times 10^{-4}$	$1.1470 \times 10^{-2}$	$4.7271 \times 10^{-2}$
$\alpha_8$	—	$2.4804 \times 10^{-4}$	$4.2804 \times 10^{-3}$	$2.3013 \times 10^{-2}$
$\alpha_9$	—	$5.8537 \times 10^{-5}$	$1.5080 \times 10^{-3}$	$1.0627 \times 10^{-2}$
$\alpha_{10}$	—	$1.3103 \times 10^{-5}$	$5.0452 \times 10^{-4}$	$4.6761 \times 10^{-3}$
$\alpha_{11}$	—	—	$1.6103 \times 10^{-4}$	$1.9683 \times 10^{-2}$

Figure 1. Singular functions  $u_k$  for gaussian illumination with  $c = \pi$ . Near each singular function the corresponding singular value is given.

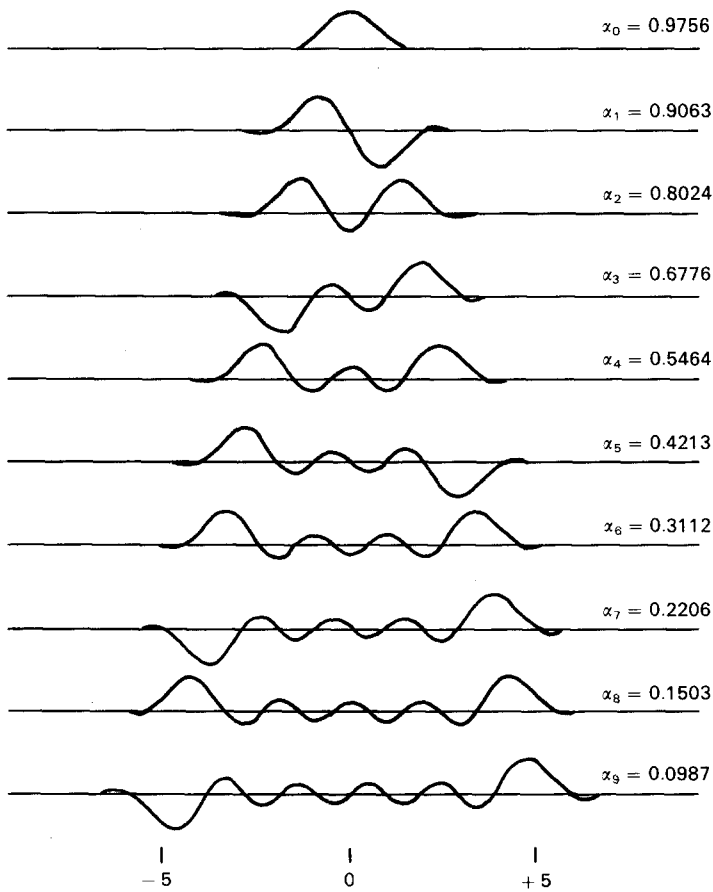


Figure 2. Singular functions  $u_k$  for gaussian illumination with  $c=2\pi$ . Near each singular function the corresponding singular value is given.

distance between adjacent zeros decreases slowly for increasing  $k$  since the space interval in which  $u_k$  is large is also increasing. It follows that the improvement in resolution is weakly dependent on the number of singular functions used in the inversion procedure.

For sinc illumination, an important simplification appears when the illuminating system has the same aperture as that of the imaging system. From equations (2.1) and (1.4) it follows that the corresponding integral operator is

$$(Af)(x) = \int_{-\infty}^{+\infty} \frac{\sin[\Omega(x-y)]}{\pi(x-y)} \operatorname{sinc}(\Omega y) f(y) dy \quad (5.1)$$

and, by a change of variables, it follows that if we denote by  $\alpha_k(\Omega)$  the singular values of  $A$  for an arbitrary aperture  $\Omega$ , and by  $\alpha_k$  the singular values when  $\Omega=\pi$ , then

$$\alpha_k(\Omega) = \frac{\pi}{\Omega} \alpha_k. \quad (5.2)$$

Therefore the dependence of the singular values on  $\Omega$  is trivial and we can consider only the aperture  $\Omega = \pi$ , since half the distance between the zeros of the central lobe in the illumination profile always coincides with the Rayleigh distance of the imaging system.

We have computed the singular values of the operator (5.1) using various truncations of the integral corresponding to 1, 2, 4, 8 and 16 zeros in the illumination profile to the right of the central point. Even and odd singular functions are always computed separately, as in [3]. The first four singular values rapidly converge and are already stable when truncation corresponds to the fourth zero of the sinc function.

In figure 3 are shown the singular functions of the operator (5.1) computed using eight zeros of the sinc profile. We note the same effects as those found for gaussian illumination: the moving away from the central region of the main lobes of the singular functions for increasing  $k$ , and also the 'saturation' of the zeros in the central region. Again, even if we increase the number of singular functions used in an

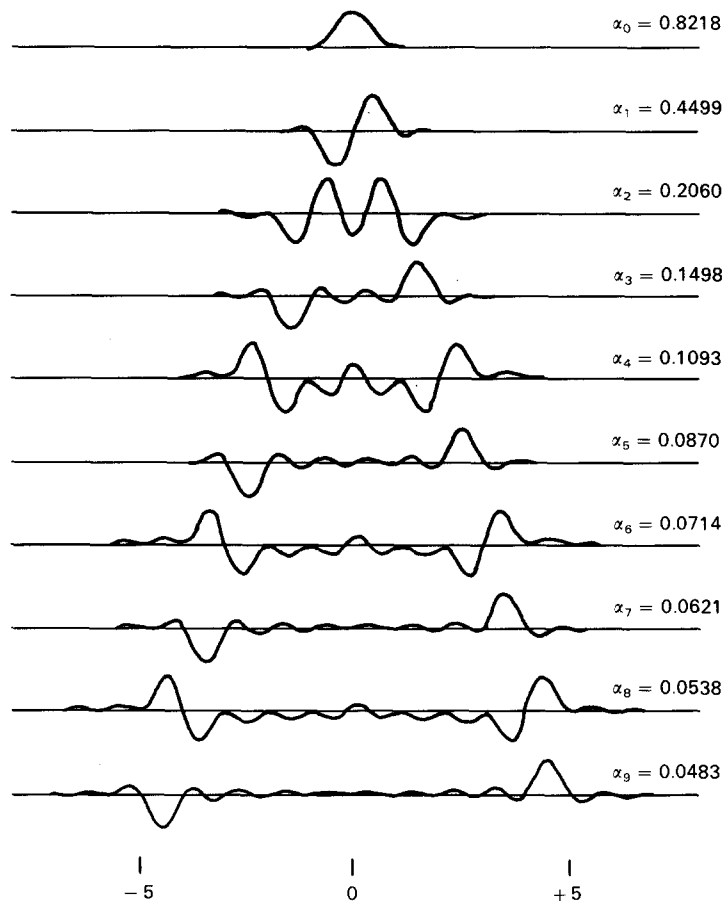


Figure 3. Singular functions  $u_k$  for sinc illumination. Near each singular function the corresponding singular value is given.

inversion procedure, we achieve no improvement in resolution beyond that obtained just by using the first few singular functions.

The behaviour exhibited by the singular functions plotted in figures 2 and 3 deserves some further consideration. If we look at the odd singular functions  $u_{2m+1}$ , figure 3 suggests that each of them has a main lobe, for  $x > 0$ , in the interval  $(m, m + 1)$  and that

$$u_{2(m+1)+1}(x) \simeq u_{2m+1}(x - 1) \tag{5.3}$$

for  $x > 0$ , while for  $x < 0$

$$u_{2(m+1)+1}(x) \simeq u_{2m+1}(x + 1). \tag{5.4}$$

These relations, which show a surprising analogy between the behaviour of the singular function of varying index and the behaviour of the solutions of a wave equation, can be verified as follows. If we write the integral equation for  $u_{2m+1}(x)$ ,  $x > 0$ , using the symmetry property and the ‘experimental’ property that  $u_{2m+1}(x)$  is large only in the interval  $(m, m + 1)$ , then

$$u_{2m+1}(x) \simeq \frac{1}{\alpha_{2m+1}^2} \int_m^{m+1} \text{sinc}(\pi x) \{ \text{sinc}[\pi(x - y)] - \text{sinc}[\pi(x + y)] \} \text{sinc}(\pi y) u_{2m+1}(y) dy. \tag{5.5}$$

If  $m$  is large, the second term between the braces can be neglected and the ‘slowly’ varying functions  $1/x$  and  $1/y$  can be replaced by  $1/m$ . Then

$$u_{2m+1}(x) \simeq \frac{1}{\alpha_{2m+1}^2} \int_m^{m+1} \frac{\sin(\pi x)}{\pi m} \text{sinc}[\pi(x - y)] \frac{\sin(\pi y)}{\pi m} u_{2m+1}(y) dy \tag{5.6}$$

and, after translation, taking  $x$  in  $(m + 1, m + 2)$ , changing the variable in the integral and reintroducing the functions  $1/x$  and  $1/y$ , we obtain

$$u_{2m+1}(x - 1) \simeq \frac{1}{\alpha_{2m+1}^2} \left( \frac{m + 1}{m} \right)^2 \int_{m+1}^{m+2} \text{sinc}(\pi x) \text{sinc}[\pi(x - y)] \times \text{sinc}(\pi y) u_{2m+1}(y - 1) dy. \tag{5.7}$$

Therefore  $u_{2m+1}(x - 1)$  is approximately a solution of the eigenvalue equation with an associated singular value given by

$$\alpha_{2(m+1)+1} \simeq \frac{m}{m + 1} \alpha_{2m+1}. \tag{5.8}$$

The corresponding relation for even singular functions is

$$\alpha_{2(m+1)} \simeq \frac{m}{m + 1} \alpha_{2m}. \tag{5.9}$$

An inspection of the values reported in figure 3 shows that these relations are in a surprisingly good agreement with the computed values: adjacent even and odd singular values satisfy equations (5.7) and (5.6) within a relative error which is not greater than 6 per cent.

Similar considerations can be applied to gaussian illumination.

**6. The two-dimensional problem**

Here we extend the theoretical results derived in §2 to two dimensions. We denote by  $S(\mathbf{x})$ ,  $\mathbf{x} = \{x_1, x_2\}$ , the point-spread function of the imaging system:

$$S(\mathbf{x}) = \frac{1}{(2\pi)^2} \iint_Q \hat{S}(\boldsymbol{\omega}) \exp [i(\mathbf{x}, \boldsymbol{\omega})] d\boldsymbol{\omega}, \tag{6.1}$$

where  $Q$  is the bounded domain in Fourier space corresponding to the frequencies transmitted by the system. For an aberration-free imaging system  $\hat{S}(\boldsymbol{\omega}) = 1$ , while if there are phase aberrations  $\hat{S}(\boldsymbol{\omega}) = \exp [i\alpha(\boldsymbol{\omega})]$ , with  $\alpha(\boldsymbol{\omega})$  real-valued. Furthermore, we denote by  $P(\mathbf{x})$  the profile of the illuminating beam in the object plane. We assume, as in §2, that the profile function satisfies the conditions

$$|P(\mathbf{x})| \leq 1 \tag{6.2}$$

and

$$\iint_{-\infty}^{+\infty} |P(\mathbf{x})|^2 d\mathbf{x} < +\infty. \tag{6.3}$$

These conditions are satisfied both by the gaussian profile

$$P(\mathbf{x}) = \exp\left(-\frac{\rho^2}{2\beta^2}\right), \quad \rho = \sqrt{x_1^2 + x_2^2} \tag{6.4}$$

and by the band-limited profile

$$P(\mathbf{x}) = 2 \frac{J_1(\Omega\rho)}{\Omega\rho}, \quad \rho = \sqrt{x_1^2 + x_2^2}. \tag{6.5}$$

For the latter profile, condition (6.3) follows from the well-known asymptotic behaviour

$$\frac{2J_1(\Omega\rho)}{\Omega\rho} \sim \pi \left(\frac{2}{\pi\Omega\rho}\right)^{3/2} \sin\left(\Omega\rho - \frac{\pi}{4}\right), \quad \rho \rightarrow \infty. \tag{6.6}$$

Under these conditions the basic operator describing the imaging system is given by

$$(Af)(\mathbf{x}) = \iint_{-\infty}^{+\infty} S(\mathbf{x} - \mathbf{y})P(\mathbf{y})f(\mathbf{y}) d\mathbf{y}, \tag{6.7}$$

and this is analogue, in two dimensions, of the operator (2.1).

When the profile function satisfies condition (6.3) the operator  $A$  is compact in  $L^2(\mathfrak{R}^2)$ . Indeed, from Parseval equality, for both aberration-free imaging and for phase aberrations (in both cases  $|\hat{S}(\boldsymbol{\omega})| = 1$ ) we see that the kernel of  $A$  is square-integrable and hence  $A$  is a Hilbert-Schmidt operator. Then

$$\begin{aligned} \iint_{-\infty}^{+\infty} d\mathbf{x} \iint_{-\infty}^{+\infty} d\mathbf{y} |S(\mathbf{x} - \mathbf{y})|^2 |P(\mathbf{y})|^2 &= \left(\iint_{-\infty}^{+\infty} |S(\mathbf{x})|^2 d\mathbf{x}\right) \left(\iint_{-\infty}^{+\infty} |P(\mathbf{y})|^2 d\mathbf{y}\right) \\ &= \left(\frac{1}{(2\pi)^2} \iint_Q |\hat{S}(\boldsymbol{\omega})|^2 d\boldsymbol{\omega}\right) \left(\iint_{-\infty}^{+\infty} |P(\mathbf{y})|^2 d\mathbf{y}\right) = \frac{\Sigma(Q)}{(2\pi)^2} \iint_{-\infty}^{+\infty} |P(\mathbf{y})|^2 d\mathbf{y} < +\infty \end{aligned} \tag{6.8}$$

where  $\Sigma(Q)$  denotes the area of the aperture of the imaging system. Furthermore, as with the operator (2.1), one can prove that the operator (6.7) is not injective when  $\hat{P}(\omega)$  has a bounded support (as with the profile function (6.5)) and that it is injective when  $\hat{P}(\omega)$  is analytic (as with the profile function (6.4)).

Since the adjoint operator  $A^*$  is given by

$$(A^*g)(\mathbf{y}) = \iint_{-\infty}^{+\infty} P^*(\mathbf{y})S^*(\mathbf{x}-\mathbf{y})g(\mathbf{x}) d\mathbf{x}, \tag{6.9}$$

the singular system  $\{\alpha_k; u_k, v_k\}_{k=0}^{+\infty}$  of  $A$  is the set of solutions of the coupled equations

$$\iint_{-\infty}^{+\infty} S(\mathbf{x}-\mathbf{y})P(\mathbf{y})u_k(\mathbf{y}) d\mathbf{y} = \alpha_k v_k(\mathbf{x}) \tag{6.10}$$

$$\iint_{-\infty}^{+\infty} P^*(\mathbf{y})S^*(\mathbf{x}-\mathbf{y})v_k(\mathbf{x}) d\mathbf{x} = \alpha_k u_k(\mathbf{y}). \tag{6.11}$$

As usual, when the operators  $A$  and  $A^*$  are injective, both  $\{u_k\}_{k=0}^{+\infty}$  and  $\{v_k\}_{k=0}^{+\infty}$  are orthogonal bases in  $L^2(\mathfrak{R}^2)$ ; otherwise these sets form orthogonal bases in the orthogonal complements of the null spaces of  $A$  and  $A^*$ , respectively.

From equations (6.10) and (6.11) it follows that the singular functions  $v_k$  are band-limited, while the singular functions  $u_k$  are generally not (except when the profile function is also band-limited). Properties of the singular functions analogous to those derived in §2 hold in the absence of aberrations. Indeed, in such a case the point-spread function  $S(\mathbf{x})$  satisfies the conditions

$$S^*(\mathbf{x}) = S(-\mathbf{x}) \tag{6.12}$$

and

$$\iint_{-\infty}^{+\infty} S(\mathbf{x}-\mathbf{y})S(\mathbf{y}) d\mathbf{y} = S(\mathbf{x}); \tag{6.13}$$

furthermore,  $S(\mathbf{x}-\mathbf{y})$  is the kernel of the projection operator over the subspace of the functions having a Fourier transform supported in  $Q$ . Then, from equation (6.11)

$$u_k(\mathbf{y}) = \frac{1}{\alpha_k} P^*(\mathbf{y})v_k(\mathbf{y}), \tag{6.14}$$

from which there follows the double orthogonality property

$$\iint_{-\infty}^{+\infty} v_k(\mathbf{y})v_j^*(\mathbf{y}) d\mathbf{y} = \delta_{kj}, \tag{6.15}$$

$$\iint_{-\infty}^{+\infty} |P(\mathbf{x})|^2 v_k(\mathbf{x})v_j^*(\mathbf{x}) d\mathbf{x} = \alpha_k^2 \delta_{kj}, \tag{6.16}$$

which is an extension of the double orthogonality of the generalized prolate spheroidal functions obtained by Slepian [16].

The singular functions  $u_k$  can also be obtained as eigenfunctions of the integral operator

$$(A^*Af)(\mathbf{x}) = \iint_{-\infty}^{+\infty} P^*(\mathbf{x})S(\mathbf{x}-\mathbf{y})P(\mathbf{y})f(\mathbf{y}) d\mathbf{y} \tag{6.17}$$

associated with the eigenvalues  $\alpha_k^2$ . The numerical solution of this eigenvalue problem is easy only for a square pupil

$$S(\mathbf{x}) = \frac{\sin(\Omega x_1)}{\pi x_1} \frac{\sin(\Omega x_2)}{\pi x_2}, \quad (6.18)$$

provided the profile function  $P(\mathbf{x})$  takes the form

$$P(\mathbf{x}) = P_1(x_1)P_2(x_2). \quad (6.19)$$

Note that this condition is satisfied by the gaussian profile (6.4) or by the band-limited profile

$$P(\mathbf{x}) = \text{sinc}(\Omega x_1) \text{sinc}(\Omega x_2), \quad (6.20)$$

but not by the band-limited 'circular' profile (6.5). For imaging described by equations (6.18) and (6.19), the two-dimensional eigenvalue problem can be reduced to the solution of two one-dimensional eigenvalue problems: the singular values of the two-dimensional problem are given by the product of the singular values of the one-dimensional problems, and the two-dimensional singular functions by the tensor product of the one-dimensional singular functions. This is just the analogue of the problem of a square pupil and square object discussed on [1].

For a circular pupil, when the point-spread function is given by

$$S(\mathbf{x}) = \frac{\Omega}{2\pi} \frac{J_1(\Omega\rho)}{\rho}, \quad \rho = \sqrt{(x_1^2 + x_2^2)} \quad (6.21)$$

and the profile function is also a function of  $\rho$  (this condition is satisfied by both profiles (6.4) and (6.5)), the two-dimensional eigenvalue problem can be reduced to an infinite set of one-dimensional eigenvalue problems. More precisely, the singular functions  $u_k(\mathbf{x})$  can be expressed in the form

$$u_{n,m}(\mathbf{x}) = \frac{1}{\rho} \phi_{n,m}(\Omega; \rho) \exp(im\phi), \quad n=0, \pm 1, \pm 2, \dots, \quad m=0, 1, 2, \dots \quad (6.22)$$

(where  $\{\rho, \phi\}$  are the polar coordinates of the point  $\{x_1, x_2\}$ ) and the functions  $\phi_{n,m}(\Omega, \rho)$  are solutions of the eigenvalue problems

$$\int_{-\infty}^{+\infty} \sqrt{(\rho\rho')} P^*(\rho) K_n(\Omega; \rho, \rho') P(\rho') \phi_{n,m}(\Omega; \rho') d\rho' = \alpha_{n,m}^2 \phi_{n,m}(\Omega; \rho), \quad (6.23)$$

where

$$K_n(\Omega; \rho, \rho') = \int_0^\Omega \omega J_n(\omega\rho) J_n(\omega\rho') d\omega. \quad (6.24)$$

Furthermore, the singular functions  $v_k(\mathbf{x})$  can be derived from equation (6.14).

The extension to sampled data can be carried out along the lines described in [3].

## 7. Application to scanning microscopy

It was indicated in [1] that the theory of singular systems in diffraction-limited imaging would have implications in microscopy. With the detailed results obtained in the previous sections of this paper, we may now consider this question in some depth. We have seen that resolution beyond the usual Rayleigh limit may be expected if prior knowledge of the support of the object is available and, in

particular, if this support is reduced to the order of size of the wavelength used. This is precisely the situation which obtains in the conventional acoustic or optical scanning microscope. The imaging system of such a microscope, termed type II by Sheppard and Choudhury [17], is shown in figure 4. Here the object support can be assumed to be defined by the profile of the focused incident radiation. If the input lens is uniformly illuminated and of the same aperture as the imaging lens, equations (1.1) and (1.4) apply; thus, the full image is given by

$$g(x) = \int_{-\infty}^{\infty} \frac{\sin[\Omega(x-y)]}{\pi(x-y)} \operatorname{sinc}(\Omega y) f(y) dy. \tag{7.1}$$

We consider for simplicity the one-dimensional problems; the extension to two dimensions follows procedure described in § 6.

A translation of the specimen by  $-\zeta$  gives a new image,

$$g_{\zeta}(x) = \int_{-\infty}^{\infty} \frac{\sin[\Omega(x-y)]}{\pi(x-y)} \operatorname{sinc}(\Omega y) f(y + \zeta) dy. \tag{7.2}$$

In the type II microscope we record the image at  $x=0$ , say  $G(\xi) = g_{\xi}(0)$ , so that, ignoring any detector integration,

$$G(\xi) = \int_{-\infty}^{\infty} \frac{\sin^2(\Omega y)}{\pi\Omega y^2} f(y + \xi) dy \tag{7.3}$$

or, with a change of variable,

$$\begin{aligned} G(x) &= \int_{-\infty}^{\infty} \frac{\sin^2[\Omega(x-y)]}{\pi\Omega(x-y)^2} f(y) dy \\ &= \int_{-\infty}^{\infty} S(x-y) f(y) dy, \end{aligned} \tag{7.4}$$

where the ‘amplitude’ point-spread function is

$$S(x) = \frac{\sin^2(\Omega x)}{\pi\Omega x^2}, \tag{7.5}$$

which is the same as the intensity point-spread function for an incoherently illuminated ordinary microscope or type I scanning microscope.

To apply the singular system theory to microscopy we must try to reconstruct the ‘super-resolved’ object, within its given support, by recording the full image and projecting it onto the image-plane singular functions to find the coefficients of the object-plane singular functions, as described in [1]–[3].

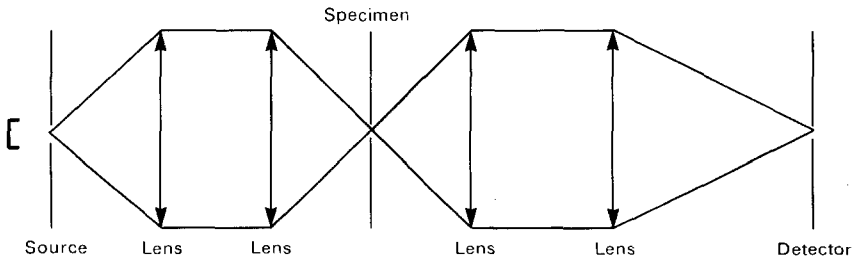


Figure 4. Schematic diagram of a type II scanning microscope.

The addition of a multiplicity of detectors to a conventional type II microscope, as suggested in [1], will produce an instrument whose response may be calculated as follows. We work in the singular function basis to reconstruct the object at each scanning position  $\xi$ . If the microscope is optical, we assume also that some means has been used to find the image phase as discussed in [1]; the phase will be available directly in the acoustic case. The reconstructed object is then given by

$$\tilde{f}_\xi(x) = \sum_{k=0}^N \frac{1}{\alpha_k} (g_k, v_k) u_k(x), \quad (7.6)$$

where  $N+1$  is the number of singular functions used. We assume as usual that

$$g = Af + n, \quad (7.7)$$

where  $n$  represents an additive noise contribution, so that

$$\begin{aligned} (g, v_k) &= (Af, v_k) + (n, v_k) \\ &= \alpha_k (f, u_k) + (n, v_k). \end{aligned} \quad (7.8)$$

Thus

$$\tilde{f}_\xi(x) = \sum_{k=0}^N u_k(x) \int_{-\infty}^{\infty} u_k(y) f(y + \xi) dy + \text{noise term}. \quad (7.9)$$

We now use the value of the reconstructed object at  $x=0$  and write  $f_r(\xi) = \tilde{f}_\xi(0)$ . Then, dropping noise terms,

$$f_r(\xi) = \sum_{k=0}^N u_k(0) \int_{-\infty}^{\infty} u_k(y) f(y + \xi) dy \quad (7.10)$$

or, with a change of variable,

$$f_r(x) = \int_{-\infty}^{\infty} S(x-y) f(y) dy, \quad (7.11)$$

where the amplitude response function is now

$$S(x) = \sum_{k=0}^N u_k(0) u_k(x). \quad (7.12)$$

In §2 we proved in the case of the sinc profile function that the singular functions  $u_k$  are a basis in the space of band-limited functions, with band  $[-2\Omega, 2\Omega]$ , which are zero at the sampling points  $n\pi/\Omega$  ( $n = \pm 1, \pm 2, \dots$ ). It follows that

$$\sum_{k=0}^{\infty} u_k(x) u_k(y) = \frac{\pi}{2\Omega} \frac{\sin(2\Omega x)}{\pi x} \frac{\sin(2\Omega y)}{\pi y} + \sum_{\text{odd}} \frac{\sin 2\Omega(x - (n\pi/2\Omega)) \sin 2\Omega(y - (n\pi/2\Omega))}{\pi(x - (n\pi/2\Omega)) \pi(y - (n\pi/2\Omega))} \quad (7.13)$$

By putting  $y=0$  in equation (7.13) we find that in the limit  $N = \infty$ , equation (7.12) becomes  $S(x) = \sin(2\Omega x)/(\pi x)$ . We see, therefore, that the performance of the new microscope approaches that of a type I coherent microscope of twice the resolving power. The number of terms  $N$  required to approach this limit is not large since the singular functions of higher order, as may be seen in figure 3, only add to the wings of the response. Figure 5 shows equation (7.12) taken to ten terms, together with its Fourier transform (the Fourier transform of the response of the type II scanning microscope covers the band  $[-2\Omega, 2\Omega]$  in a triangular fashion).

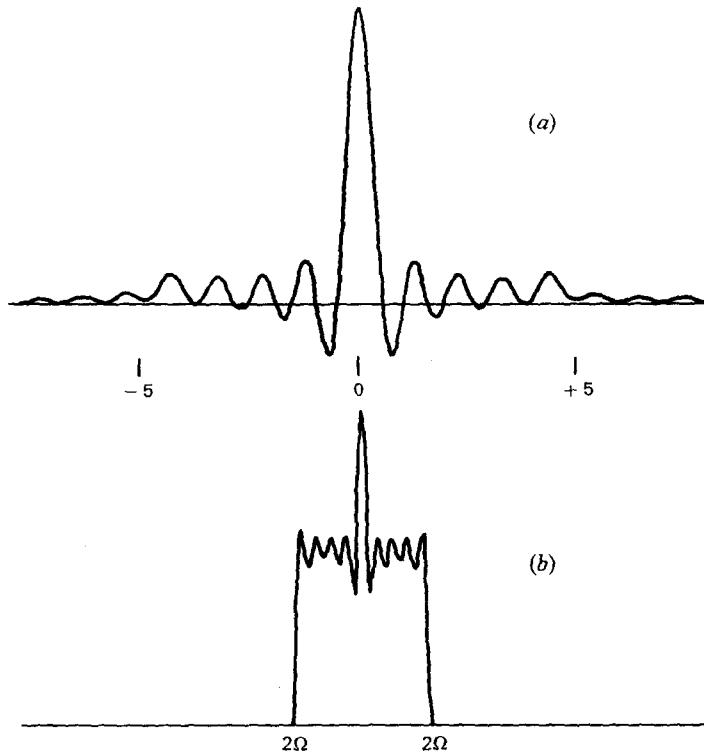


Figure 5. Amplitude point-spread function (a) and corresponding Fourier transform (b) of new scanning microscope with singular value reconstruction of image data.

A further possibility with this new microscope is to use the entire reconstruction of equation (7.9) at each scanning point, followed by averaging at each object point. The response function for this mode of operation may also be calculated.

From equation (7.9) we have that

$$\tilde{f}_{\xi}(x-\xi) = \int_{-x}^x \sum_{k=0}^N u_k(x-\xi)u_k(y)f(y+\xi) dy \quad (7.14)$$

or, with a change of variable,

$$\tilde{f}_{\xi}(x-\xi) = \int_{-\infty}^{\infty} \sum_{k=0}^N u_k(x-\xi)u_k(y-\xi)f(y) dy. \quad (7.15)$$

Averaging over object points gives

$$\begin{aligned} F(x) &= \int_{-\infty}^{\infty} \left( \sum_{k=0}^N \int_{-\infty}^{\infty} u_k(x-\xi)u_k(y-\xi) d\xi \right) f(y) dy \\ &= \int_{-x}^{\infty} S_1(x-y)f(y) dy \end{aligned} \quad (7.16)$$

where

$$\begin{aligned} S_1(x) &= \sum_{k=0}^N \int_{-\infty}^{\infty} u_k(x+\eta)u_k(\eta) d\eta \\ &= \sum_{k=0}^N (u_k \otimes u_k)(x), \end{aligned} \quad (7.17)$$

where  $\otimes$  denotes autocorrelation and subscript I denotes integration.

In figure 6, equation (7.17) is shown taken to ten terms, also with its Fourier transform.

As  $N \rightarrow \infty$  we may again use the result (7.13) to find that

$$S_I(x) = \text{const} \times \frac{\sin(2\Omega x)}{\pi x} \quad (7.18)$$

which, in a photon-limited regime, will give a gain in signal amplitude to noise of the order of the square root of the number of integrated image points since the constant is proportional to the length of the image. So far in this section we have considered the extra performance achievable when the object support is provided by band-limited illumination; greater increases in resolution are possible if a hard aperture of the order of a wavelength is used in the object plane or if an object support of this dimension is defined by its self-luminosity or fluorescence, and the possible increases in resolution are as described in [1].

Work is in progress to put the above schemes into practice at the limits of optical resolution, but results have already been published [18] which demonstrate the extra information available in an optical imaging instrument when using these principles.

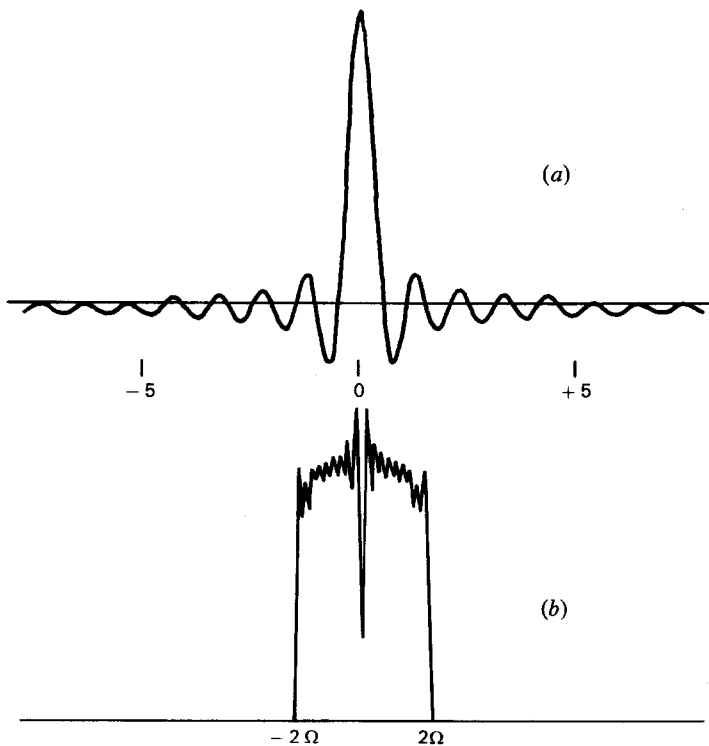


Figure 6. As figure 5, but with integration as described in equation (7.16).

### Acknowledgments

We are grateful to Dr. Fred Brackenhoff for discussions on the techniques of scanning microscopy and to Professor Charles McCutchen for helpful correspondence. We are also indebted to Professor F. Gori for stimulating and very helpful discussions. Dr. C. De Mol is Research Associate with the National Fund for Scientific Research (Belgium).

Le précédent travail de cette série, dans lequel la théorie des systèmes singuliers a été utilisée pour discuter le problème de l'imagerie à la limite de diffraction, est généralisé pour permettre la reconstruction d'un objet sur une région qui contient des contours 'doux'. La généralisation est introduite pour s'occuper de faisceaux gaussiens ou d'autres éclairages ou encore des connaissances a priori incertaines de position. Les solutions sont développées dans un espace pondéré  $L^2$ . Des exemples de fonctions et vecteurs singuliers, sous éclairage à la fois gaussien et sinc, sont donnés. L'analyse est appliquée pour déterminer les fonctions de réponse en amplitude de systèmes de microscopes à balayage optique ou acoustique proposés par Bertero et Pike dans le premier article de la série et on trouve que les performances du microscope à balayage de type nouveau devraient s'approcher exactement de celles d'un microscope cohérent conventionnel de deux fois le pouvoir de résolution.

### References

- [1] BERTERO, M., and PIKE, E. R., 1982, *Optica Acta*, **29**, 727.
- [2] BERTERO, M., BOCCACCI, P., and PIKE, E. R., 1982, *Optica Acta*, **29**, 1599.
- [3] BERTERO, M., BRIANZI, P., PARKER, P., and PIKE, E. R., 1984, *Optica Acta*, **31**, 181.
- [4] TORALDO DI FRANCIA, G., 1969, *J. opt. Soc. Am.*, **59**, 799.
- [5] BERTERO, M., BOCCACCI, P., and PIKE, E. R., 1982, *Proc. R. Soc. A*, **383**, 15.
- [6] BERTERO, M., BOCCACCI, P., and PIKE, E. R., 1984, *Proc. R. Soc. A*, **393**, 51.
- [7] BERTERO, M., BRIANZI, P., and PIKE, E. R., 1984, *Proc. R. Soc. A* (in the press).
- [8] MCCUTCHEN, C. W., 1967, *J. opt. Soc. Am.*, **57**, 1190.
- [9] LUTTRELL, S., 1983, Private communication.
- [10] GORI, F., and PALMA, G., 1975, *J. Phys. A*, **8**, 1709.
- [11] KAC, M., MURDOCK, W. L., and SZEGÖ, G., 1953, *J. rat. Mech. Analysis*, **2**, 767.
- [12] LANDAU, H. J., 1975, *J. analyse Math.*, **28**, 335.
- [13] SLEPIAN, D., 1965, *J. Math. Phys.*, **44**, 99.
- [14] PAPOULIS, A., 1966, *Proc. Inst. elect. electron. Engrs*, **54**, 947.
- [15] FRIEDEN, B. R., 1971, *Progress in Optics*, Vol IX, edited by E. Wolf (Amsterdam: North Holland), p. 311.
- [16] SLEPIAN, D., 1964, *Bell Syst. tech.J.*, **43**, 3009.
- [17] SHEPPARD, C. J. R., and CHOUDHURY, A., 1977, *Optica Acta*, **24**, 1051.
- [18] WALKER, J. G., 1983, *Optica Acta*, **30**, 1197.